Int. J. Solids Structures, 1971, Vol. 7, pp. 399 to 417. Pergamon Press. Printed in Great Britain

APPLICATION OF VARIABLE MODULI MODELS TO SOIL BEHAVIOR†

IVAN NELSON‡ and MELVIN L. BARON§

Paul Weidlinger, Consulting Engineer, New York

Abstract—A mathematical material model is described in which the basic constitutive law is an isotropic relation between the increments of stress and strain. No unique stress–strain relation, *per se*, exists. Neither is there an explicit yield condition. The bulk and shear moduli, however, are functions of the stress and/or strain invariants.

The behavior of two simple models of this type is examined for the two generally available soil tests, i.e. uniaxial strain and triaxial compression. In each case qualitative agreement with the behavior of real soils is obtained. For one model, unloading and reloading is also considered.

The latter model is also compared with a simple elastic–plastic model. Many similarities between the two become apparent, but so do significant differences, e.g. the direction of the "plastic" strain increment.

NOTATION

c_1, c_2, c_3	constants
E	Young's modulus
e	mean strain
e_0	initial mean strain in triaxial test
e_{ij}	components of deviatoric strain tensor
e_1, e_2, e_3	principal deviatoric strains
G	shear modulus
G_0	initial shear modulus
G_{UN}	shear modulus in unloading
h	step function
J_2'	second invariant of stress deviator
K	bulk modulus
K_0, K_1, K_2	constants appearing in bulk modulus
K_{LD}, K_{UN}	bulk modulus in loading, unloading
k	constant related to cohesion
p	pressure
s_{ij}	components of deviatoric stress tensor
s_1, s_2, s_3	principal deviatoric stresses
u_i	components of particle velocity
α	coefficient in Prager–Drucker yield condition
β	constant, $2(1+\nu_0)/(1-2\nu_0)$
$\gamma_1, \bar{\gamma}_1$	constants in combined variable shear modulus
δ_{ij}	Kronecker delta
$\Delta\varepsilon_1$	measured axial strain in triaxial test
ε_{ij}	components of strain tensor
$\varepsilon_1, \varepsilon_2, \varepsilon_3$	principal strains
ε_{kk}	volumetric strain, $3e$
ν	Poisson's ratio

† This paper is the result of studies sponsored by the U.S. Army Engineer Waterways Experiment Station, Vicksburg, Mississippi.

‡ Senior Research Engineer.

§ Partner and Adjunct Professor of Civil Engineering, Columbia University.

ν_0	Poisson's ratio at zero stress and strain
ξ	variable of integration
σ_{ij}	components of stress tensor
$\sigma_1, \sigma_2, \sigma_3$	principal stresses
ϕ	angle of internal friction of granular material

1. INTRODUCTION

EARLY attempts to mathematically model the behavior of soils under both static and or dynamic loadings were based on the assumption that the soil could be approximated by a linear elastic material. Such models were of course of extremely limited validity. They were subsequently replaced by relatively simple elastic–plastic models of the von Mises or Prager–Drucker, Ref. [1], type in which a yield condition was used to describe the material failure under specific combinations of the shear stresses and pressure. At the same time, nonlinear elastic models were considered, e.g. Ref. [2], but these also were not too successful. More recently, in connection with the study of ground shock effects from explosive sources, a series of more advanced elastic–plastic models have been used to model the action of the soil over a rather wide variation of applied pressures, Refs. [3–5]. In these models the yield condition depended upon the pressure in a general way and arbitrary nonlinear pressure–volume relations were used. Different pressure–volume relations were used for initial loading and for subsequent unloading and reloading. The various stages in the historical development of these advanced elastic–plastic models are described in Ref. [3]. Generally, these models reproduce actual soil behavior quite adequately in both static and dynamic uniaxial strain tests. However, as pointed out in Ref. [3], they do not reproduce the behavior in triaxial compression tests. Although the elastic ideally plastic models (nonstrain hardening) may give the proper failure stress for a triaxial test, they do not give the correct stress–strain behavior of the material as it approaches failure.

The present study is concerned with the development of mathematical models which contain no explicit yield condition, but which have bulk and shear moduli which are functions of the invariants of the stress and or strain tensors. The behavior of two simple models of this type are examined for the two generally available soil tests, i.e. uniaxial strain and triaxial compression. In each case qualitative agreement is obtained with the behavior of real soils.

Finally, the second model is compared with a simple elastic–plastic model. Many similarities between the models become apparent, but there are also significant differences which are discussed.

2. MODEL DESCRIPTION

1. *General conditions*

The mathematical description of the model is in terms of the incremental stress–strain relations

$$s_{ij} = 2G\dot{e}_{ij} \tag{1}$$

$$\dot{\sigma} = 3K\dot{\theta} \tag{2}$$

where s_{ij} and e_{ij} are the deviatoric stress and strain, respectively, and p and e† are the mean stress and strain. In writing equation (1) relating the increments of deviatoric stress and strain, an implicit assumption is made that the material is isotropic. Of course, real soils, being the results of largely directional geological processes, are often anisotropic. Moreover, the separation of the constitutive relation into deviatoric and volumetric parts, while particularly convenient, automatically precludes any coupling between them as is observed in certain granular media. However, for the applications described in Section 1, equations (1) and (2) will be considered a sufficiently accurate material description.

Both the shear modulus and the bulk modulus will be assumed to depend upon the stress and or strain invariants. In general, different functions G and K apply in initial loading and subsequent unloading and reloading. The present discussion will be largely confined to the case of initial loading.

It is noted that, even in cases of initial loading, there is not in general a unique stress–strain relation. The final state of strain depends not only upon the final state of stress, but also upon the stress path used to reach the final state. In this sense, the variable moduli material cannot be considered a nonlinear elastic material where such a unique stress–strain relation would exist.

The description of a material in terms of incremental stress–strain relations has been termed a "hypo-elastic material", Refs. [6 and 7]. The present variable moduli material may be considered a special case of an isotropic hypo-elastic material in which the tensor relating stress and strain increments depends on the invariants, but not on the stress (or strain) tensor itself. Of course, the present material is in general irreversible even for incremental loading.

In writing equations (1) and (2) the strain rate is well defined as the deformation rate tensor

$$\dot{\varepsilon}_{ij} = \tfrac{1}{2}(u_{i,j} + u_{j,i}) \tag{3}$$

even for large strains. For dynamic problems with large rotations Jaumann's definition of the stress rate, Ref. [6], should be used. In a general numerical scheme this could be done. In this paper, however, small strains and rotations as well as quasi-static loading will be assumed.

A particular model will be discussed from the standpoint of the uniaxial strain and triaxial compression tests, since these are the soil tests which are generally available. Typical experimental curves for each test are shown in Fig. 1. Other examples may be seen in Refs. [8 and 9].

The stress–strain curve in the uniaxial strain case, Fig. 1(a), typically (but not always) shows a reversal in curvature on loading. On unloading, the slope is almost constant and is much larger than the slope during initial loading, except for a sharp tail in the low stress range. Reloading, except for a small hysteresis loop, generally follows the unloading curve up to the previous maximum stress, and then continues along the initial loading curve. The lateral stress σ_3, required to maintain uniaxial strain, is sometimes also measured, Fig. 1(b).

† In this paper compressive stress and strain are defined as positive in accordance with the usual Soil Mechanics Convention.

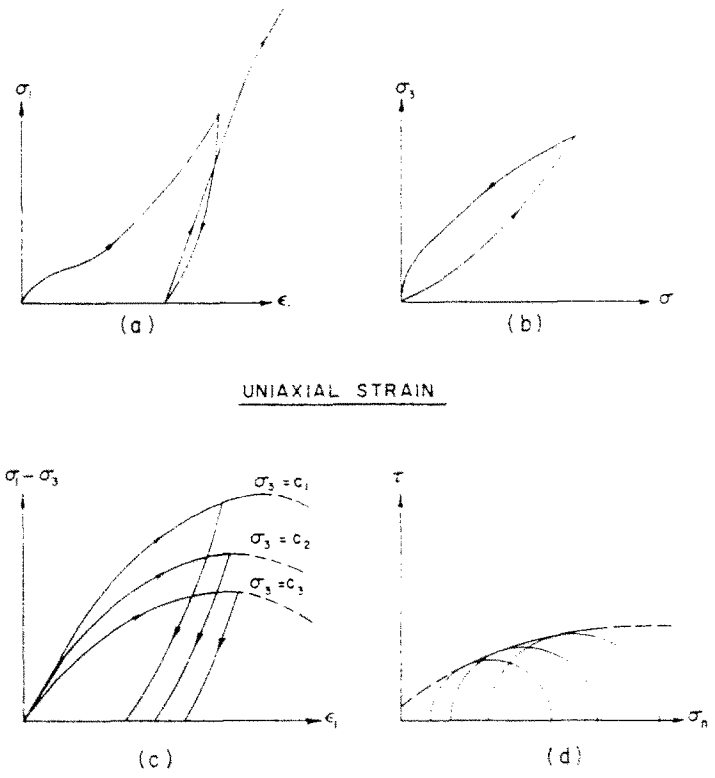

FIG. 1 Typical experimental results.

Typical experimental triaxial results, Fig. 1(c), have the following characteristics:

1. The stress–strain curve at a given value of σ_3 is concave downward.
2. At some point a horizontal tangent, "failure", is reached.
3. At a higher value of σ_3 the initial slope and the stress difference at failure, $(\sigma_1 - \sigma_3)_{max}$, both increase.

Unloading and reloading information in triaxial compression is often not available. Existing data indicates that if unloading (before failure) occurs, the unloading curve is much steeper than the loading curve. There is some question, however, concerning the behavior of soils in the triaxial configuration during reloading.

By plotting the Mohr's circles at failure for different lateral stresses σ_3, the Mohr envelope, Fig. 1(d), is obtained. This envelope is generally either a straight line (for some dry sands) or is concave downward (for partially saturated soils).

In Ref. [3] the models were discussed from the standpoint of the two tests: one in which K and G were both functions of the strain invariants, and a second model in which K depended upon the volumetric strain but where G depended upon the stress invariants. Both models exhibited the salient features of both tests. In the present paper only the latter, or the combined stress–strain variable moduli model, is discussed.

2. *Combined stress–strain variable moduli model*

The combined stress–strain variable moduli model is defined (in initial loading) by a bulk modulus K which is a function of the mean strain e, and a shear modulus G which is a function of first two stress invariants, or more specifically the pressure p and the square root of the second invariant of the stress deviator $\sqrt{J_2'}$. The simplest such relations which satisfy the test results described in Section 1 are

$$K = K(e) = K_0 + K_1 e + K_2 e^2 \tag{4}$$

$$G = G(p, \sqrt{J_2'}) = G_0 + \gamma_1 p + \bar{\gamma}_1 \sqrt{J_2'}. \tag{5}$$

Equations (4) and (5) may be thought of as the first terms in the series expansions of more general analytic functions K and G of the stress and strain invariants. The quantity $\sqrt{J_2'}$ was used, rather than J_2' itself, since it is of the same order as p and the components of the stress tensor. At zero stress and strain, the bulk and shear moduli reduce respectively to K_0 and G_0, the "linear elastic" values, which are related in terms of the "elastic" Poisson's ratio ν_0

$$\frac{K_0}{G_0} = \frac{2(1+\nu_0)}{3(1-2\nu_0)} = \frac{\beta}{3} \tag{6}$$

although the ratio K/G is not, in general, constant. With γ_1 positive and $\bar{\gamma}_1$ negative, the material hardens in shear with increasing pressure and softens with increasing shear stress.

The bulk modulus was chosen to be a quadratic in e rather than in p, since the typical uniaxial strain test curve suggests that the axial stress is a cubic function of the axial strain. Since the bulk modulus K refers to the incremental pressure–volumetric strain relation,

$$\dot{p} = 3K\dot{e} \qquad \text{[See equation (2)]}$$

the pressure may be obtained by direct integration of equation (2) as

$$p = \int_0^e 3K(\xi)\,\mathrm{d}\xi = 3K_0 e + \tfrac{3}{2}K_1 e^2 + K_2 e^3. \tag{7}$$

Since for initial loading, the pressure is a monotonic function of e, a unique inverse $e(p)$ exists. Thus, the bulk modulus K may also be written as

$$K = K(p) = K[e(p)]. \tag{8}$$

Therefore, equation (4) is equivalent to writing K as a function of p.

(a) *Uniaxial strain.* By using stress symmetry and vanishing of two of the principal strain rates, it may be shown that in uniaxial strain

$$\frac{\mathrm{d}\sigma_1}{\mathrm{d}e} = 3K + 4G = 3[K_0 + K_1 e + K_2 e^2] + 4[G_0 + \gamma_1 p + \bar{\gamma}_1 \sqrt{J_2'}]. \tag{9}$$

Noting that

$$\sqrt{J_2'} = \frac{\sqrt{3}}{2} s_1 = \frac{\sqrt{3}}{2}(\sigma_1 - p),$$

substitution of equation (7) into equation (9) yields the first order nonhomogeneous differential equation

$$\frac{d\sigma_1}{de} - 2\sqrt{(3)}\bar{\gamma}_1\sigma_1 = (3K_0 + 4G_0) + 3\left[4K_0\left(\bar{\gamma}_1 - \frac{\sqrt{3}}{2}\bar{\gamma}_1\right) - K\right]e$$
$$- 3\left[2K_1\left(\bar{\gamma}_1 - \frac{\sqrt{3}}{2}\bar{\gamma}_1\right) + K_2\right]e^2 + 4K_2\left(\bar{\gamma}_1 - \frac{\sqrt{3}}{2}\bar{\gamma}_1\right)e^3 \tag{10}$$

Using the initial condition that stress and strain vanish simultaneously, the solution for stress as an explicit function of strain is found by integrating equation (10)

$$\sigma_1 = -\left\{\frac{2G_0}{\sqrt{(3)}\bar{\gamma}_1} + \frac{\bar{\gamma}_1}{\bar{\gamma}_1^2}\left[K_0 + \frac{K_1}{2\sqrt{(3)}\bar{\gamma}_1} + \frac{2K_2}{(2\sqrt{(3)}\bar{\gamma}_1)^2}\right]\right\}\{1 - \exp(2\sqrt{(3)}\bar{\gamma}_1 e)\}$$
$$-\left\{\frac{2\sqrt{(3)}K_0}{\bar{\gamma}_1}\left(\bar{\gamma}_1 - \frac{\sqrt{3}}{2}\bar{\gamma}_1\right) + \frac{\bar{\gamma}_1}{\bar{\gamma}_1^2}\left(K_1 + \frac{K_2}{\sqrt{(3)}\bar{\gamma}_1}\right)\right\}e$$
$$-\left\{\frac{\sqrt{(3)}K_1}{\bar{\gamma}_1}\left(\bar{\gamma}_1 - \frac{\sqrt{3}}{2}\bar{\gamma}_1\right) + \frac{\bar{\gamma}_1}{\bar{\gamma}_1^2}K_2\right\}e^2 - \frac{2K_2}{\sqrt{(3)}\bar{\gamma}_1}\left(\bar{\gamma}_1 - \frac{\sqrt{3}}{2}\bar{\gamma}_1\right)e^3 \tag{11}$$

Closed form expressions for the remaining stress quantities, s_1 and σ_3, are easily obtainable from equations (7) and (11).

$$s_1 = -\left\{\frac{2G_0}{\sqrt{(3)}\bar{\gamma}_1} + \frac{\bar{\gamma}_1}{\bar{\gamma}_1^2}\left[K_0 + \frac{K_1}{2\sqrt{(3)}\bar{\gamma}_1} + \frac{2K_2}{(2\sqrt{(3)}\bar{\gamma}_1)^2}\right]\right\}\{1 - \exp(2\sqrt{(3)}\bar{\gamma}_1 e)\}$$
$$-\left[\frac{2\sqrt{(3)}\bar{\gamma}_1}{\bar{\gamma}_1}K_0 + \frac{\bar{\gamma}_1}{\bar{\gamma}_1^2}\left(K_1 + \frac{K_2}{\sqrt{(3)}\bar{\gamma}_1}\right)\right]e$$
$$-\left[\frac{\sqrt{(3)}\bar{\gamma}_1}{\bar{\gamma}_1}K_1 + \frac{\bar{\gamma}_1}{\bar{\gamma}_1^2}K_2\right]e^2 - \frac{2\bar{\gamma}_1}{\sqrt{(3)}\bar{\gamma}_1}K_2e^3 \tag{12}$$

$$\sigma_3 = \left\{\frac{G_0}{\sqrt{(3)}\bar{\gamma}_1} + \frac{\bar{\gamma}_1}{2\bar{\gamma}_1^2}\left[K_0 + \frac{K_1}{2\sqrt{(3)}\bar{\gamma}_1} + \frac{2K_2}{(2\sqrt{(3)}\bar{\gamma}_1)^2}\right]\right\}\{1 - \exp(2\sqrt{(3)}\bar{\gamma}_1 e)\}$$
$$+\left[\frac{\sqrt{(3)}K_0}{\bar{\gamma}_1}(\bar{\gamma}_1 + \sqrt{(3)}\bar{\gamma}_1) - \frac{\bar{\gamma}_1}{2\bar{\gamma}_1^2}\left(K_1 + \frac{K_2}{\sqrt{(3)}\bar{\gamma}_1}\right)\right]e$$
$$+\left[\frac{\sqrt{(3)}K_1}{2\bar{\gamma}_1}(\bar{\gamma}_1 + \sqrt{(3)}\bar{\gamma}_1) + \frac{\bar{\gamma}_1}{2\bar{\gamma}_1^2}K_2\right]e^2 - \frac{K_2}{\sqrt{(3)}\bar{\gamma}_1}(\bar{\gamma}_1 + \sqrt{(3)}\bar{\gamma}_1)e^3 \tag{13}$$

Finally, from equation (11), the slope of the stress–strain curve at any point, or the tangent (constrained) modulus is found to be

$$\frac{d\sigma_1}{de_1} = \frac{14}{13}G_0 - \frac{2\bar{\gamma}_1}{\sqrt{(3)}\bar{\gamma}_1}\left[K_0 + \frac{K_1}{2\sqrt{(3)}\bar{\gamma}_1} + \frac{2K_2}{(2\sqrt{(3)}\bar{\gamma}_1)^2}\right]\exp(2\sqrt{(3)}\bar{\gamma}_1 e)$$
$$-\frac{2K_0}{\sqrt{(3)}\bar{\gamma}_1}\left(\bar{\gamma}_1 - \frac{\sqrt{3}}{2}\bar{\gamma}_1\right) - \frac{\bar{\gamma}_1}{3\bar{\gamma}_1^2}\left(K_1 + \frac{K_2}{\sqrt{(3)}\bar{\gamma}_1}\right)$$
$$-\left[\frac{2K_1}{\sqrt{(3)}\bar{\gamma}_1}\left(\bar{\gamma}_1 - \frac{\sqrt{3}}{2}\bar{\gamma}_1\right) + \frac{2\bar{\gamma}_1}{3\bar{\gamma}_1^2}K_2\right]e - \frac{2K_2}{\sqrt{(3)}\bar{\gamma}_1}\left(\bar{\gamma}_1 - \frac{\sqrt{3}}{2}\bar{\gamma}_1\right)e^2 \tag{14}$$

(b) *Triaxial stress.* In the triaxial stress configuration the second invariant of the stress deviators is simply related to the stress difference by

$$\sqrt{J_2} = \frac{\sqrt{3}}{2} s_1 = \frac{1}{\sqrt{3}}(\sigma_1 - \sigma_3). \tag{15}$$

Using the relation $p = (\sigma_1 + 2\sigma_3)/3$ and equation (15), the expression for the shear modulus becomes

$$G = G_0 + \frac{\gamma_1}{3}(\sigma_1 + 2\sigma_3) + \frac{\bar{\gamma}_1}{\sqrt{3}}(\sigma_1 - \sigma_3). \tag{16}$$

Thus, the strain deviator e_1 may be found by integration

$$e_1 = \int \frac{ds_1}{2G} = \int_{\sigma_3}^{\sigma_1} \frac{d\xi}{3G_0 + \sigma_3(2\gamma_1 - \sqrt{(3)}\bar{\gamma}_1) + \xi(\gamma_1 + \sqrt{(3)}\bar{\gamma}_1)} \tag{17}$$

since $e_1 = 0$ when $\sigma_1 = \sigma_3$ (hydrostatic compression). From equation (17), e_1 is obtained as an explicit function of the stresses σ_1 and σ_3

$$e_1 = \frac{1}{\gamma_1 + \sqrt{(3)}\bar{\gamma}_1} \ln \left[\frac{3G_0 + \sigma_3(2\gamma_1 - \sqrt{(3)}\bar{\gamma}_1) + \sigma_1(\gamma_1 + \sqrt{(3)}\bar{\gamma}_1)}{3(G_0 + \gamma_1\sigma_3)} \right]. \tag{18}$$

A necessary condition for G to decrease as σ_1 increases, see equation (16), is

$$\gamma_1 + \sqrt{(3)}\bar{\gamma}_1 < 0 \tag{19}$$

so that the argument of the logarithmic function in equation (18) is always less than one, and e_1 is always positive. Alternatively, equation (18) may be written as

$$e_1 = \frac{1}{\gamma_1 + \sqrt{(3)}\bar{\gamma}_1} \ln \left[\frac{G}{G_{\text{initial}}} \right] \tag{20}$$

where $G_{\text{initial}} = G_0 + \gamma_1\sigma_3$ is the initial value of G, i.e. the value under hydrostatic conditions. From equation (20), it is evident that e_1 becomes arbitrarily large (as does ε_1) as G approaches zero, or [from equation (16)] when

$$(\sigma_1 - \sigma_3)_{\max} = -\frac{3(G_0 + \gamma_1\sigma_3)}{\gamma_1 + \sqrt{(3)}\bar{\gamma}_1}. \tag{21}$$

It is seen that for $(\sigma_1 - \sigma_3)$ larger than $(\sigma_1 - \sigma_3)_{\max}$, the strain becomes imaginary, that is, the strain cannot exist. Thus, equation (21) expresses the maximum stress difference in triaxial compression for a given lateral stress σ_3. It should also be noted that the slope of the triaxial stress–strain curve

$$\frac{d\sigma_1}{d\varepsilon_1} = \frac{9KG}{3K + G} \equiv E\dagger \tag{22}$$

i.e. the local Young's modulus, goes to zero when $G \to 0$, so that the stress difference $(\sigma_1 - \sigma_3)_{\max}$ represents a point of horizontal tangency, i.e. "failure".

† It can be shown that equation (22) applies for quite general functions, K and G.

The measured strain $\Delta\varepsilon_1$ is simply related to the strain deviator e_1, the mean strain e, and the initial (hydrostatic) mean strain e_0 by

$$\Delta\varepsilon_1 = e_1 + e - e_0 \tag{23}$$

where e_0 is found for the given lateral stress σ_3 by solving equation (7) for $e = e_0$ with $p = \sigma_3$. Equations (4), (5), (18), (22), (23) and the small positive root e of the cubic equation (7) completely define the system in triaxial stress for all valid states σ_1, $\sigma_3[(\sigma_1 - \sigma_3) < (\sigma_1 - \sigma_3)_{max}]$.

If the Mohr failure envelope were plotted for this material, it is evident from equation (21) that the plot would be a straight line passing above the origin, similar to the yield condition for a Prager–Drucker material. This similarity will be discussed later in the paper.

(c) *Choice of constants.* If all stress quantities are nondimensionalized with respect to the initial bulk modulus, K_0, then five parameters remain to fully describe the model, namely,

$$\frac{G_0}{K_0}, \frac{K_1}{K_0}, \gamma_1, \bar{\gamma}_1, \frac{K_2}{K_0}. \tag{24}$$

The first of these is inherently positive and is related to the initial Poisson's ratio ν_0 by equation (6). The higher order terms in the bulk modulus K_1/K_0 and K_2/K_0 may be positive or negative. However, the values are restricted by the condition $K > 0$. If K_1 were negative and K_2 positive, the requirement that the minimum bulk modulus be positive requires that

$$K_2 > \frac{K_1^2}{4K_0} \tag{25}$$

The fact that $\gamma_1 > 0$ and $\bar{\gamma}_1 < 0$ for physical reasons has already been discussed, as has the inequality between them, equation (19).

To further restrict the range of the five material parameters, one requires the initial slope in triaxial compression to increase with lateral stress. Differentiating equation (22) with respect to σ_3

$$\frac{1}{9}\frac{dE}{d\sigma_3} = \frac{3K^2(dG\ d\sigma_3) + G^2(dK\ d\sigma_3)}{(3K+G)^2} \tag{26}$$

and requiring the result to be positive when $\sigma_1 = \sigma_3$, yields the inequality

$$9\gamma_1^2[K_0 + K_1 e_0 + K_2 e_0^2]^{2/3} + [G_0 + \gamma_1(3K_0 e_0 + \tfrac{3}{2}K_1 e_0^2 + K_2 e_0^3)]^2(K_1 + 2K_2 e_0) > 0. \tag{27}$$

For equation (27) to hold in the limit as e_0 approaches zero the inequality

$$\gamma_1 > -\frac{1}{9}\left(\frac{G_0}{K_0}\right)^2\left(\frac{K_1}{K_0}\right) \tag{28}$$

must be satisfied. Equation (28) is a necessary condition for the initial slope in the triaxial test to increase with increasing lateral stress σ_3.

If the initial curvature in the uniaxial strain test were negative, then the condition

$$\frac{K_1}{K_0} < -\frac{4}{3\bar{\gamma}_1}\left[2\frac{G_0}{K_0} + \frac{3}{2}\gamma_1\right] \tag{29}$$

must be satisfied.

Equation (29) is obtained by evaluating the derivative of equation (14) at $e = 0$. An attempt to find an analytic expression for the inflection point leads to a transcendental equation and will not be discussed further.

(d) *Unloading and reloading.* The model for unloading and subsequent reloading of variable moduli materials is presently at an early stage of development. Experimentally, Fig. 1(a), the uniaxial strain unloading curve has a slope much larger than the loading slope, which is approximately constant until very low stress levels are reached. Reloading generally follows the unloading curve up to a point close to the previous maximum stress. If the stress is increased further, the stress–strain curve approaches the continuation of the original loading curve.

In a completely general three dimensional configuration the terms "loading" and "unloading" no longer have such clear cut meanings. It is possible that the material will be loading in shear ($\dot{J}_2' > 0$) and unloading in pressure ($\dot{p} < 0$) simultaneously. In fact, if one studies the $\sigma_3 - \sigma_1$ curve for as simple a geometry as a uniaxial strain test, Fig. 1(b), it can be shown that on unloading, the deviator $s_1 = \frac{2}{3}(\sigma_1 - \sigma_3)$ (originally positive) first decreases, then changes sign and continues to decrease (increases negatively) until a minimum is reached at a very low stress level. Beyond this point, s_1 appears to increase slightly, i.e. to decrease in absolute value. At the same time, the pressure $p = (\sigma_1 + 2\sigma_3)/3$ and the strain ε_1 both decrease monotonically during unloading. Clearly, the sharp tails found experimentally upon unloading at very low stress levels in both the uniaxial stress–strain curve, Fig. 1(a), and the radial stress–axial stress curve, Fig. 1(b), are related to this unusual behavior of s_1. Elastic–plastic models in which the yield condition is a function of the pressure can adequately represent this behavior, Ref. [3].†

In classical plasticity, both ideal and hardening, the terms "loading" and "unloading" are uniquely defined by the change in stresses relative to the current yield condition. When different loading and unloading pressure–volume relations are used as in Refs. [3–5] the terms "loading" and "unloading" are no longer uniquely defined since different criteria are used for the volumetric and deviatoric portions. In an analogous manner, in the present model different criteria will be used for the volumetric and deviatoric portions.

As a first approach, the material model in unloading was chosen to be defined by the following expressions for the bulk and shear moduli:

$$K = K_{UN} = \text{const.} \tag{30}$$

$$G = G_{UN} = G_0 + \gamma_1 p + \bar{\gamma}_1 \sqrt{(J_2')} h(\dot{J}_2') \tag{31}$$

where $h(\dot{J}_2')$ is the unit step function. The unloading bulk modulus K_{UN} is used whenever the pressure is decreasing $\dot{p} < 0$ (unloading) or whenever $\dot{p} > 0$ but the pressure is less than the maximum previous pressure $p < p_{\max}$ (reloading).

The effect of the step function in equation (31) is that at the same values of p and J_2', the material is stiffer in shear when it is unloading *in shear*, $\dot{J}_2' < 0$, than when it is loading in shear, $\dot{J}_2' > 0$. This insures that in an incremental loading–unloading cycle there is energy dissipation. It is not clear that $\dot{J}_2'$ should be the criterion upon which the choice of the proper G is based. Further study may indicate that some combination of $\dot{J}_2'$ and $\dot{p}$ should be used for this purpose.

† It can be shown that the minimum value of the deviator s_1 occurs when upon unloading, the opposite face of the yield surface is reached. Upon continued unloading, the stress path is along the yield surface.

With the present description of unloading, equations (30) and (31), the slope of the uniaxial stress–strain curve in unloading, $K_{UN}+\frac{4}{3}G_{UN}$, could not be less than K_{UN} unless G_{UN} were permitted to be negative for some range of stresses. This, of course, is objectionable on other grounds. Thus, in order to obtain the sharp break found in the experimental curve, Fig. 1(a), at low stress levels, some other material description, possibly involving coupling between deviatoric and volumetric effects, is required.

For the present model, K_{UN} must be chosen larger than the maximum value of K found during loading. A second requirement is that $\frac{3}{2}K_{UN}$ must be greater than the maximum value of G_{UN}.† A detailed description of the equations applicable to unloading will not be given.

(e) *Numerical results.* Typical results for the variable moduli model of this section are shown in Figs. 2–5. The parameters used in the computations were $\nu_0 = 0{\cdot}30$, $K_1/K_0 = -100$, $K_2/K_0 = 4000$, $\gamma_1 = 60$ and $\bar{\gamma} = -133{\cdot}3$. In loading, the uniaxial stress–strain curve, Fig. 2, has the characteristic reversal of curvature which is often found in experimental curves. Again, the point of inflection occurs at a strain close to 4 per cent, a typical value. On unloading, with $K_{UN}/K_0 = 30$, the stress decreases sharply. Although the unloading portion appears to be a straight line, the slope at low stress levels is in fact less than half the value at high stress levels. Nevertheless, the distinct tail which is found on unloading experimentally, Fig. 1(a), does not appear, illustrating the inadequacy of the present unloading model at these very low stresses.

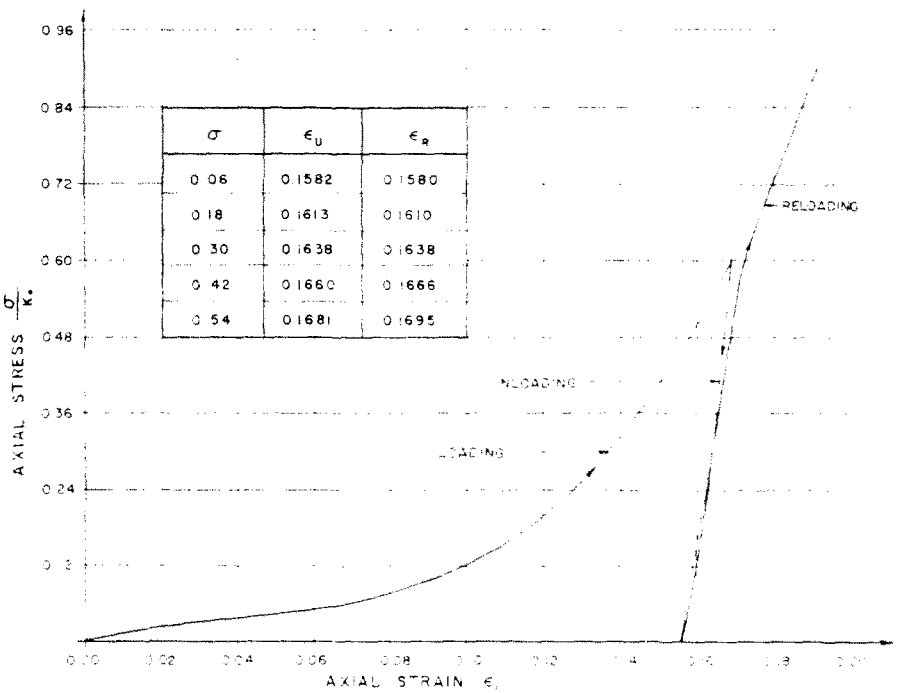

FIG. 2. Stress–strain relation in uniaxial strain. Variable moduli mixed model. $K = K_0 + K_1(\nu - \nu_0) + K_2(\nu - \nu_0)^2$; $G = G_0 + \gamma_1(\nu - \nu_0) + \bar{\gamma}(J_2)$ drawn for $\nu_0 = 0{\cdot}30$, $K_1/K_0 = -100$, $K_2/K_0 = 4000$, $\gamma_1 = 60$, $\bar{\gamma} = -133{\cdot}3$, $K_{UN}/K_0 = 30$.

† This corresponds to the requirement $\ldots > 0$.

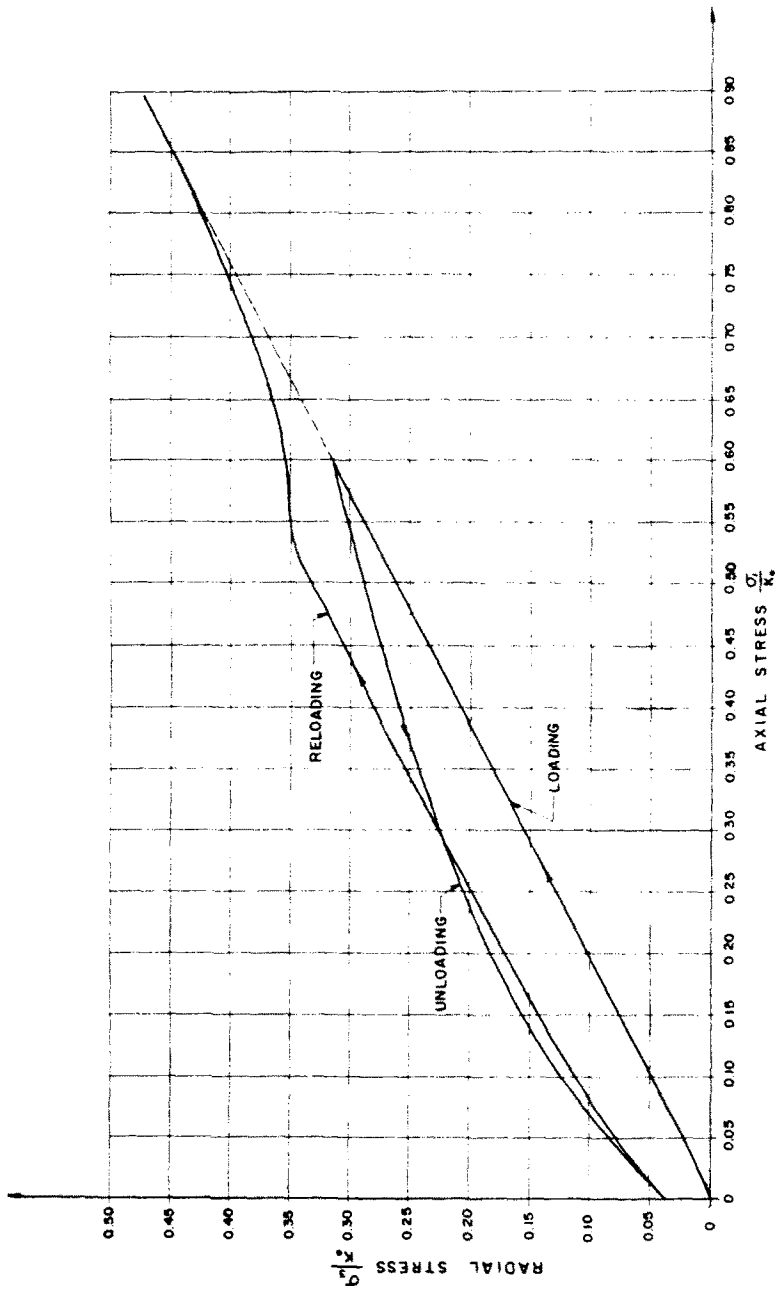

FIG. 3. Radial stress vs. axial stress in uniaxial strain. Variable moduli mixed model, $K = K_0 + K_1 e + K_2 e^2$; $G = G_0 + \gamma_1 P + \gamma_2 \sqrt{J_2}$ (*drawn for* $\nu_0 = 0.30$, $K_1/K_2 = -100$, $K_2/K_0 = 4000$, $\gamma_1 = 60$, $\gamma_2 = -133.3$, $K_{UN}/K_0 = 30$).

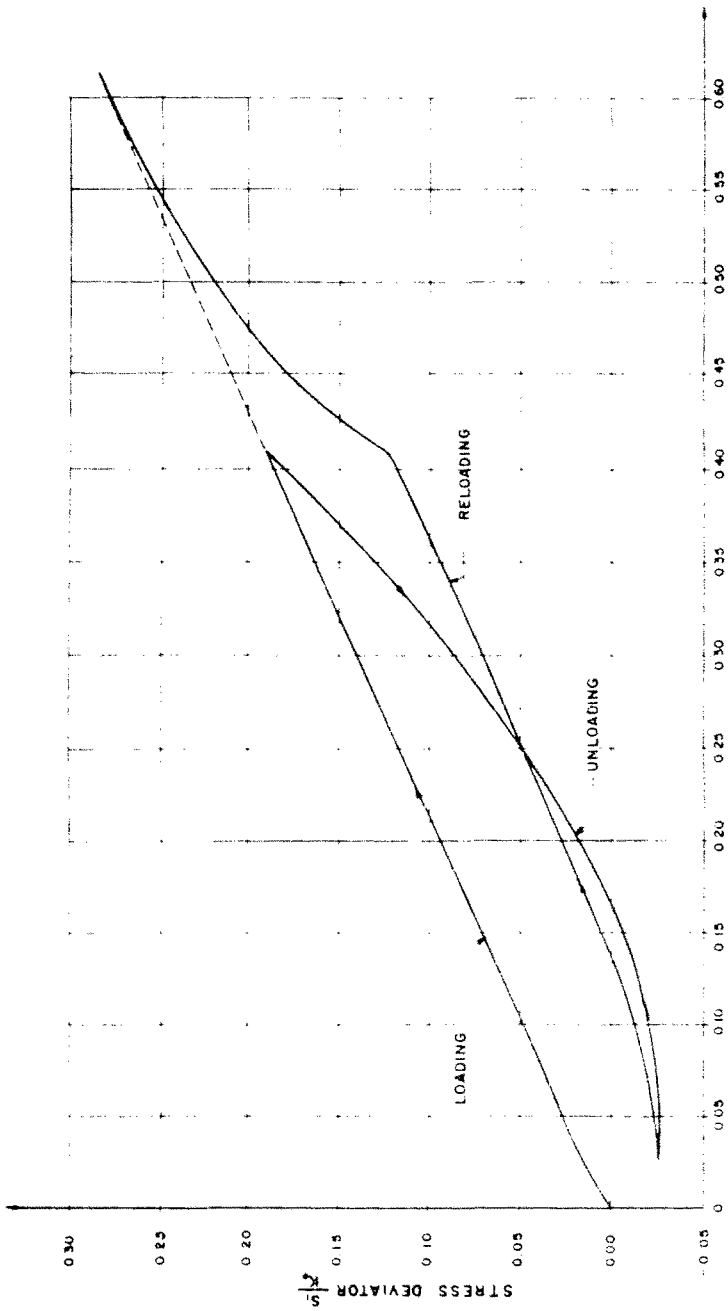

Fig. 4. Stress deviator vs. pressure in uniaxial strain. Variable moduli mixed model, $K = K_0 + K_1\varepsilon + K_2\varepsilon^2$; $G = G_0 + G_1 p + G_2 p^2$; J_2 (drawn for $\varepsilon = 0.40$, $K_1/K_0 = 100$, $K_2/K_0 = 400$, $G_1/G_0 = 60$, $G_2/G_0 = 133.3$, $K_{1S}/K_0 = 30$).

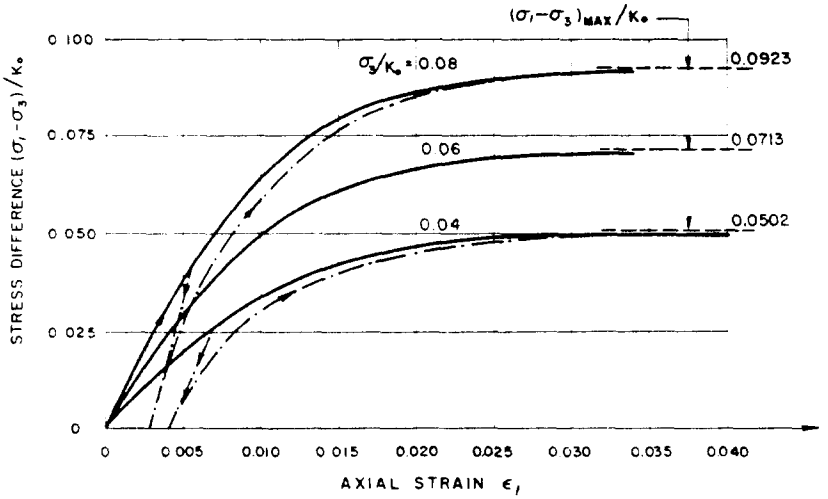

FIG. 5. Triaxial compression test. Variable moduli mixed model. $K = K_0 + K_1 e + K_2 e^2$; $G = G_0 + \gamma_1 p + \bar{\gamma}_1 \sqrt{J_2'}$ (drawn for $\nu_0 = 0{\cdot}30$, $K_1/K_0 = -100$, $K_2/K_0 = 4000$, $\gamma_1 = 60$, $\bar{\gamma}_1 = -133{\cdot}3$).

Upon reloading, the initial slope is greater than the final unloading slope since now $\dot{J}_2 < 0$. A small hysteresis loop is thus formed. The reloading curve crosses the unloading curve and approaches the continuation of the initial loading curve as the stress increases. The table on Fig. 2 is enclosed to distinguish the unloading and reloading curves. If, instead of increasing the load above the previous maximum, cyclic loading were to take place, loops similar to the one shown would be produced.

The plot of the radial stress versus axial stress in uniaxial strain is shown in Fig. 3. On unloading, the curve is actually concave upward at very low stress levels. At higher stresses, the curve is essentially a straight line. The unloading radial stress is always greater than the corresponding value in loading. The unloading curve is concave downward and changes in curvature at $\sigma_1/K_0 = 0{\cdot}164$, where s_1/K_0 changes sign. The plot has the same general characteristics as the experimental curves, Fig. 1(b), except that in the experimental unloading curve σ_3 drops off much more sharply as σ_1 is brought back to zero. The reloading curve is seen to approach the continuation of the initial loading curve as the stress is increased above its previous maximum value.

Finally, the deviator s_1 is plotted versus the pressure p in Fig. 4 for loading and unloading—reloading in uniaxial strain. The local slope depends only on the local value of Poisson's ratio or

$$\frac{ds_1}{dp} = \frac{4G(s_1, p)}{3K(p)} = \frac{2(1-2\nu)}{1+\nu}. \tag{32}$$

On loading, the initial curvature is concave downward. However, the major portion of the curve is essentially a straight line. On unloading s_1 is always less than its corresponding value in loading and the curve is concave upward. At $s_1 = 0$, the slope is continuous, but the curvature suddenly increases, reflecting the change in sign of $\dot{J}_2'$ in equation (31). Unloading ends at $s_1 = -p$ (so that $\sigma_1 = 0$) with the slope almost horizontal (or G almost

zero). On reloading, J_2' again becomes negative so that the new path starts out above the previous one. The slope is continuous, but the curvature discontinues, when the p-axis is crossed once more. After crossing the unloading curve, the reloading curve reaches the maximum previous pressure where the slope changes discontinuously (as K goes from K_{UN} to K_{LD}). Thereafter, the reloading curve approaches the continuation of the original loading curve.

The results for the triaxial compression test are illustrated in Fig. 5. The curves are drawn for the same parameters which were used in the uniaxial strain test and for the values of the lateral stress $\sigma_3/K_0 = 0{\cdot}04, 0{\cdot}06, 0{\cdot}08$. Each of the curves loaded directly to failure (solid) is concave downward and approaches asymptotically the value $(\sigma_1 - \sigma_3)_{max}$ given by equation (21). At a higher value of the lateral stress, the stress difference at failure increases, as does the initial slope. Also shown in Fig. 5 is the effect of unloading and reloading. Both the extreme curves were interrupted during loading, unloaded to $\sigma_1 - \sigma_3 = 0$ and reloaded to failure (the dashed curves). The loading portion, almost straight, is slightly concave upward. The reloading curves, beyond the maximum previous stress, are parallel to the virgin loading curves and approach the same asymptote. Repeated loading–unloading cycles would reproduce the same pattern each cycle; i.e. the strain would continuously increase.

On the basis of the present results, one sees that the theoretical combined variable moduli material, when subjected to two special loading configurations, namely the uniaxial strain and triaxial compression test, reproduces all† the salient features found experimentally in these tests. Therefore, the present model offers promise of being able to give a reasonable representation of real soils in more general loading configurations.

The ability of the present model to match, numerically, real soil data and the process used to determine the various constants must await the completion of current investigations.

3. COMPARISON OF VARIABLE MODULI AND PLASTIC MODELS

In the previous section, similarities between the variable moduli models and the plastic models have been mentioned. This section discusses several of these similarities for simplified models of these types. On the basis of the present study, it appears that the concepts of a "yield condition" and of "plastic flow" may be contained within the theory of the variable moduli models.

For many materials, empirical evidence suggests the existence of states of stress (and/or strain) at which the material undergoes continuously increasing deformations with little or no increase in loading. This combination of stresses at which flow occurs is often called a "flow condition" or a "yield condition". When these deformations become sufficiently large so that unacceptable changes in the geometry occur, this state is called "failure". Plastic material models describe the stress state at which flow begins by a yield condition and the subsequent deformations by a flow rule. The variable moduli models describe the behavior of materials as they approach this critical state of stress (and/or strain) as well as their behavior at the state itself.

An interesting illustration of the relation between plastic and variable moduli models can be obtained by a comparison of the simple Prager–Drucker material and the combined

† Except for the tail during unloading in uniaxial strain

variable moduli material with $K_1 = K_2 = 0$, and $K_{UN} = K_0$. For both models, the Mohr failure envelope is a straight line. In the Prager–Drucker material, permissible states of stress may be defined in terms of the yield condition, Ref. [1],

$$k + 3\alpha p - \sqrt{J_2} \geq 0. \tag{33}$$

In the combined variable moduli material, permissible states of stress are those for which $G \geq 0$, or, dividing equation (5) by $-\bar{\gamma}_1 > 0$

$$\left(\frac{G_0}{-\bar{\gamma}_1}\right) + \left(\frac{\gamma_1}{-\bar{\gamma}_1}\right) p - \sqrt{J_2} \geq 0. \tag{34}$$

The two conditions are identical if

$$\left(\frac{G_0}{-\bar{\gamma}_1}\right) = k \tag{35}$$

and

$$\left(\frac{\gamma_1}{-\bar{\gamma}_1}\right) = 3\alpha. \tag{36}$$

The requirement that $\gamma_1 + \sqrt{(3)}\bar{\gamma}_1 < 0$, equation (19), is thus equivalent to requiring that $\alpha < 1/\sqrt{3}$. There is no obvious requirement for $\gamma_1 + \sqrt{3/(2)}\bar{\gamma}_1 < 0$, which would correspond to the usual restriction on α†

$$\alpha < \frac{1}{2\sqrt{3}}. \tag{37}$$

In uniaxial strain, the requirement for initial softening, equation (29), with $K_1 = 0$ reduces to

$$2\frac{G_0}{K_0} + \sqrt{3}\frac{\gamma_1}{\bar{\gamma}_1} > 0 \tag{38}$$

which upon substitution of equation (36) and $\beta = 3(K_0/G_0)$ becomes

$$\alpha\beta < \frac{2}{\sqrt{3}}. \tag{39}$$

The identical condition must be satisfied for a Prager–Drucker material to yield in uniaxial strain.

The behavior of both the Prager–Drucker (solid) and the simplified variable moduli (dashed) materials in both triaxial compression and uniaxial strain is shown in Figs. 6–8. The triaxial test is shown in Fig. 6. Whereas both models fail at the same stress level, the variable modulus material exhibits more realistic behavior approaching failure.

The stress path, s_1 vs. p, in uniaxial strain for the two models is shown in Fig. 7. The Prager–Drucker yield surface is represented by the two straight lines

$$s_1 = \pm\frac{2}{\sqrt{3}}(k + 3\alpha p). \tag{40}$$

† Equation (37) is not an obvious requirement either; it comes either from the restriction $\phi \leq 90°$ in plane strain, or that the slope in uniaxial strain in unloading be positive.

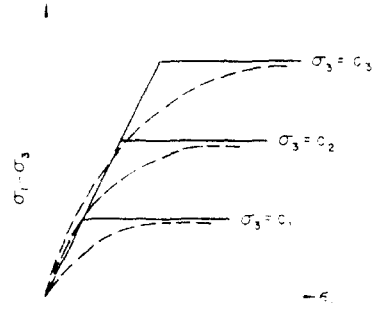

FIG. 6. Comparison of variable moduli and plastic models in triaxial compression. Solid line—Prager Drucker material (constant K and G), dashed line—combined stress-strain variable moduli model with $K_1 = K_2 = 0$.

The elastic portions of the stress path (whether loading, unloading, or reloading) have the slope $ds_1/dp = 4/3$. Unloading ceases when $\sigma_1 = s_1 + p = 0$.

In the variable moduli material, during initial loading with $K_1 = K_2 = 0$, the pressure is proportional to the mean strain, $p = 3K_0 e$, so that equation (12) for the deviator reduces to

$$s_1 = \left\{\frac{2}{\sqrt{3}}\left(\frac{G_0}{-\bar{\gamma}_1}\right) - \frac{\gamma_1 K_0}{\bar{\gamma}_1^2}\right\}\left[1 - \exp\left(\frac{2}{\sqrt{3}}\bar{\gamma}_1 \frac{p}{K_0}\right)\right] + \frac{2}{\sqrt{3}}\left(\frac{\gamma_1}{-\bar{\gamma}_1}\right)p \tag{41}$$

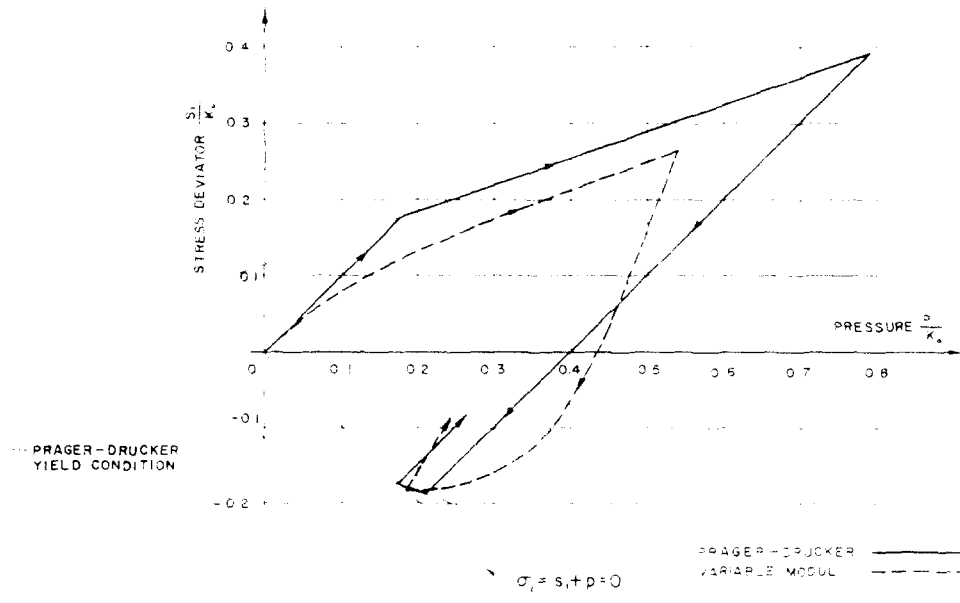

FIG. 7. Stress path in uniaxial strain. Comparison of variable moduli and Prager Drucker material (drawn for $\gamma_1 = 0.2$, $K_0 = 0.1K_{1,0}$, $K_1 = K_2 = 0$, $K_{1,0} = K_{2,0}$).

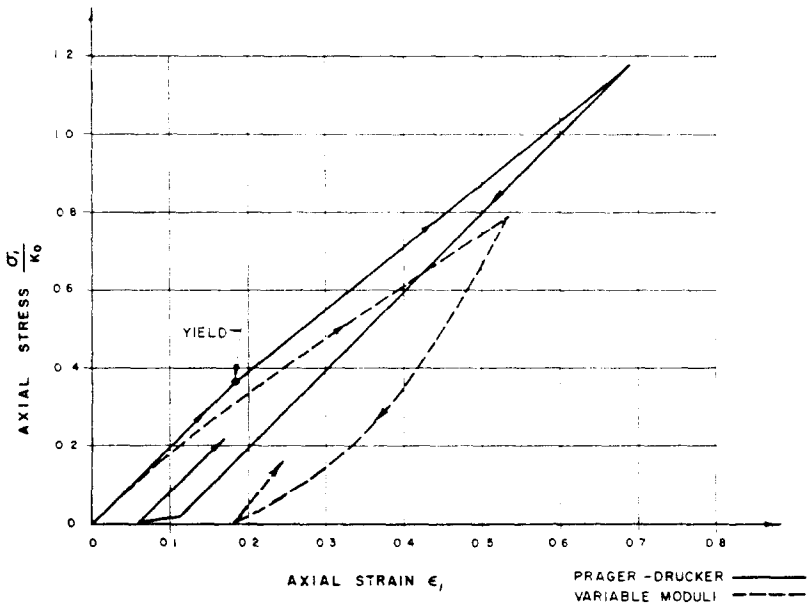

FIG. 8. Uniaxial strain test. Comparison of variable moduli and Prager–Drucker material (drawn for $\nu = 0{\cdot}2$, $k = 0{\cdot}1K_0$, $\alpha = 0{\cdot}1$, $K_1 = K_2 = 0$, $K_{UN} = K_0$).

Differentiating equation (41) with respect to p, and substituting equations (35) and (36) yields

$$\frac{ds_1}{dp} = \left[\frac{4}{\beta} - 2\sqrt{(3)}\alpha\right] \exp\left(-\frac{2\sqrt{3}}{\beta k}p\right) + 2\sqrt{(3)}\alpha \tag{42}$$

which at the origin is the elastic value and approaches the slope of the yield condition at large values of the pressure. The asymptote, although parallel to the Prager–Drucker yield condition, equation (40), is displaced by an amount

$$\Delta s_1 = -\frac{\gamma_1 K_0}{\bar{\gamma}_1^2} = -\alpha\beta k. \tag{43}$$

Unloading starts with a slope steeper than the elastic slope and approaches a horizontal tangent as the lower yield surface is neared ($G \to 0$). Reloading is again steeper than the elastic value.

Finally, the stress–strain curve in uniaxial strain is shown in Fig. 8. The Prager–Drucker curve is either elastic with slope $K_0 + \frac{4}{3}G_0$, or plastic with slope

$$\left.\frac{d\sigma_1}{d\varepsilon_1}\right]_{\text{Plastic}} = K_0 \frac{(1 \pm 2\sqrt{(3)}\alpha)^2}{(1 + 3\alpha^2\beta)} \tag{44}$$

with the upper (lower) sign applicable to the upper (lower) branches of the yield condition.

Examining the slope in uniaxial strain for initial loading for the combined mixed moduli material, equation (14), when $K_1 = K_2 = 0$, one finds

$$\frac{d\sigma_1}{d\varepsilon_1} = \left[\frac{4}{3}G_0 + \frac{2}{\sqrt{3}}\frac{\gamma_1}{\bar{\gamma}_1}K_0\right] \exp\left(\frac{2}{\sqrt{3}}\bar{\gamma}_1\varepsilon_1\right) + K_0\left(1 - \frac{2}{\sqrt{3}}\frac{\gamma_1}{\bar{\gamma}_1}\right) \tag{45}$$

The initial slope, equation (45) evaluated at $\varepsilon_1 = 0$, is the elastic constrained modulus $K_0 + \frac{4}{3}G_0$. At large strains, since $\bar{\gamma}_1 < 0$, the exponential term vanishes and the slope approaches asymptotically

$$\left.\frac{d\sigma_1}{d\varepsilon_1}\right)_{-\bar{\gamma}_1\varepsilon_1 \gg 1} = K_0\left(1 - \frac{2}{\sqrt{3}}\frac{\bar{\gamma}_2}{\bar{\gamma}_1}\right) = K_0(1 + 2\sqrt{(3)}\alpha) \tag{46}$$

which is not equal to the plastic slope, equation (44) with the positive sign. The two are equal at the end points $\alpha = 0$ and $\alpha = 2/\beta\sqrt{3}$ of the range $0 < \alpha < 2/\beta\sqrt{3}$, but the variable moduli value is slightly less than the plastic value elsewhere in the range. The value, equation (46), is that which would be obtained for a hybrid material, i.e. one which obeyed a yield condition of the Coulomb type, but obeyed a flow rule of the von Mises type, Ref. [10]. For this material there is no plastic change in volume. It is not surprising that in a material such as the variable moduli material in which the bulk modulus is a function of the mean strain only and in which shear effects cannot cause an increase in volume, the slope approaches that of the hybrid plastic material and not that of the Coulomb material itself.

The initial unloading slope is greater than the elastic value. The unloading slope decreases continuously until the minimum value K_0 is approached as G goes to zero. This is, of course, much steeper than the plastic unloading value, equation (44). The curve on reloading again starts steeper than the elastic value.

It is seen that many of the features found in elastic–plastic models are also contained in the present model. The notable difference between simple plastic models and the variable moduli model is that in the former there is a sudden yielding, or failure, while in the latter there is a gradual transition towards failure. In this respect, the present model is analogous to that proposed by Prager, Ref. [11], or to a strain or work hardening material with a null initial yield surface. The strain increments

$$\dot{e}_{ij}^{E} = \frac{1}{2G_{UN}}\dot{s}_{ij} \tag{47}$$

$$\dot{e}_{ij}^{P} = \left(\frac{1}{2G_{UN}} - \frac{1}{2G_{LD}}\right)\dot{s}_{ij} \tag{48}$$

with $G_{UN} > G_{LD}$ may be viewed as "elastic" and "plastic" parts, respectively. However, in contrast to the model in Ref. [11] and hardening plastic models where the deviatoric plastic strain increment is in the direction of the stress deviator, it is seen from equation (48) that here the deviatoric "plastic" strain increment is in the direction of the *increment* in the stress deviator. The question of which description is appropriate for soils must await more general three dimensional tests.

4. CONCLUSIONS

A theory of variable moduli materials has been partially developed in this section. The results obtained for a particular model appears to essentially match those found experimentally in both the uniaxial strain and triaxial compression tests.

Finally, the similarities and differences between the present model and plastic models are examined.

REFERENCES

[1] D. C. Drucker and W. Prager, Soil mechanics and plastic analysis or limit design. *Q. appl. Math.* 157–165 (1952).
[2] T. Y. Chang, H. Y. Ko, R. F. Scott and R. A. Westmann, An integrated approach to the stress analysis of granular materials. Report on research conducted for the National Science Foundation, California Institute of Technology (1967).
[3] I. Nelson and M. L. Baron, Investigation of ground shock effects in nonlinear hysteretic media, Report I. Development of mathematical material models. U.S. Army Engineer Waterways Experiment Station, DACA39-67-C-0048 Contract Report S-68-1, March (1968).
[4] S. S. Grigorian, On basic concepts in soil dynamics. *Physics Metals Metallogr., N.Y.* **24**, 1057–1072 (1960).
[5] I. G. Cameron and G. C. Scorgie, Dynamics of intense underground explosions. *Jnl. Inst. Math. & Applics.* **4**, 194–222 (1968).
[6] W. Prager, *Introduction to Mechanics of Continua*, Chapter VIII. Ginn (1961).
[7] C. Truesdell, Hypo-elasticity. *J. rat. Mech. Analysis* **4**, 83 (1955).
[8] R. V. Whitman, Nuclear Geoplosics, Part two—Mechanical properties of earth materials. Defense Atomic Support Agency, DASA-1285(II), May (1964).
[9] M. T. Davisson, Static and dynamic behavior of a playa silt in one-dimensional compression. Air Force Weapons Laboratory, Tech. Rpt. No. RTD TDR-63-3078, September (1963).
[10] H. H. Bleich and E. Heer, Moving step load on half-space of granular material. *Proc. Am. Soc. civ. Engrs* **89** (1963).
[11] W. Prager, On isotropic materials with continuous transition from elastic to plastic state. *Proceedings of Fifth International Congress of Applied Mechanics* (1938).

(*Received* 10 *June* 1969; *revised* 30 *March* 1970)

Абстракт—Описывается математическая модель материала, в котором основный конститутивный закон является изотропной зависимостью между приращениями напряжений и деформаций. Не существует, в основном, единственная зависимость: напряжение-деформация. Нет, даже здесь, условия пластичности в явном виде.

Модули обьема и сдвига, однако, является функциями инвариантов напряжения и, или деформации.

Исследкется поведение двух простых моделей этого типа, для двух обше доступных испытаний грунта, на пример для одноосной деформации и трехосного сжатия. Для каждого случая получается качественная сходимость с поведением дейсвительных грунтов. Для одной модели рассматривается, также, случай разгрузки и повторной нагрузки.

Последняя модель сравнивается, также, с простой упругопластической моделю. В результате исследований возникает большинство подобий между двумя моделями, но также существуют значительные разницы, например направление приращения "пластической" деформации.